Coupling of vesicle tethering and Rab binding is required for in vivo functionality of the golgin GMAP-210

Keisuke Sato*,†, Peristera Roboti*, Alexander A. Mironov, and Martin Lowe
Faculty of Life Sciences, University of Manchester, Manchester M13 9PT, United Kingdom

ABSTRACT **Golgins are extended coiled-coil proteins believed to participate in membrane-tethering events at the Golgi apparatus. However, the importance of golgin-mediated tethering remains poorly defined, and alternative functions for golgins have been proposed. Moreover, although golgins bind to Rab GTPases, the functional significance of Rab binding has yet to be determined. In this study, we show that depletion of the golgin GMAP-210 causes a loss of Golgi cisternae and accumulation of numerous vesicles. GMAP-210 function in vivo is dependent upon its ability to tether membranes, which is mediated exclusively by the amino-terminal ALPS motif. Binding to Rab2 is also important for GMAP-210 function, although it is dispensable for tethering per se. GMAP-210 length is also functionally important in vivo. Together our results indicate a key role for GMAP-210–mediated membrane tethering in maintaining Golgi structure and support a role for Rab2 binding in linking tethering with downstream docking and fusion events at the Golgi apparatus.**

Monitoring Editor
Francis A. Barr
University of Oxford

Received: Oct 14, 2014
Revised: Nov 19, 2014
Accepted: Nov 24, 2014

INTRODUCTION

The Golgi apparatus is the organelle at the heart of the eukaryotic secretory pathway and is essential for the modification and sorting of proteins and lipids (Rothman, 1981). The smallest unit of the Golgi is the cisterna, a flattened, membrane-enclosed sac. In most species, the Golgi cisternae are layered on top of each other in close apposition to form the Golgi stacks, which in vertebrate cells are laterally connected to form the Golgi ribbon (Shorter and Warren, 2002; Lowe, 2011). Many proteins have been implicated in maintaining this characteristic Golgi organization, including members of the golgin family of coiled-coil proteins (Ramirez and Lowe, 2009; Munro, 2011). Golgins are present on the cytoplasmic face of the Golgi apparatus, typically anchored at one end, and are believed to extend into the cytoplasm to facilitate efficient capture of transport vesicles or other Golgi elements. Tethering mediated by golgins is therefore believed to be important for both protein trafficking and structural organization of the Golgi apparatus. Despite this attractive hypothesis, the importance of golgin-mediated tethering in vivo remains poorly defined. It has been proposed that golgins work collectively, like tentacles, to ensure efficient capture of membranes (Sinka *et al.*, 2008; Munro, 2011) via multiple binding sites for Rab family proteins. The "tentacle" model is based on the finding that in many cases, one Rab protein can bind to multiple golgins and one golgin can bind to multiple Rab proteins, increasing efficiency of membrane capture. Implicit in this model is a high degree of redundancy between individual golgins.

GMAP-210 is a golgin localized to the *cis*-Golgi (Rios *et al.*, 1994; Cardenas *et al.*, 2009). GMAP-210 has a central coiled-coil rich region comprising 1700 residues that could extend up to 260 nm in length (Sinka *et al.*, 2008; Munro, 2011), with membrane-interacting domains at either end. At the extreme N-terminus there is a curvature-sensing amphipathic lipid-packing sensor (ALPS) motif that is able to bind to high-curvature membranes such as transport vesicles and tubules (Drin *et al.*, 2007), whereas a GRIP-related Arf binding (GRAB) domain that interacts with the GTP conformation of the small GTPase Arf1 is present at the C-terminus (Gillingham *et al.*, 2004). Because ArfGAP1 prefers high-curvature membranes

This article was published online ahead of print in MBoC in Press (http://www.molbiolcell.org/cgi/doi/10.1091/mbc.E14-10-1450) on December 3, 2014.

*These should be considered co–first authors.

†Present address: Department of Systems Neuroscience, Graduate School of Medical and Dental Sciences, Tokyo Medical and Dental University, 1-5-45, Yushima, Bunkyo-ku, Tokyo 113-8519, Japan.

Address correspondence to: Martin Lowe (martin.lowe@manchester.ac.uk).

Abbreviations used: ALPS, amphipathic lipid-packing sensor; BFA, brefeldin-A; CLEM, correlative light-electron microscopy; EM, electron microscopy; FRAP, fluorescence recovery after photobleaching; GCA, Golgicide A; GRAB, GRIP-related Arf binding; GST, glutathione S-transferase; RNAi, RNA interference.

(Bigay *et al.*, 2005), it is believed that Arf1-GTP and in turn the GRAB domain will preferentially bind to flat membranes. This led to the proposal that GMAP-210 mediates asymmetric tethering between vesicles, bound at the N-terminus by the ALPS motif, and Golgi cisternae, bound by the C-terminal GRAB domain (Drin *et al.*, 2008). The ability of mini-GMAP, comprising the ALPS motif and GRAB domain separated by a short coiled-coil region, to mediate tethering between liposomes of different curvature in vitro provides support for this model (Drin *et al.*, 2008). However, the importance of ALPS-mediated tethering has yet to be shown in vivo.

Several studies have investigated the function of GMAP-210 in vivo. Depletion of GMAP-210 in tissue culture cells was reported to cause fragmentation of the Golgi ribbon, although the stacked cisternal organization was unaffected, and there was no reduction in the rate of secretory trafficking (Rios *et al.*, 2004; Yadav *et al.*, 2009). It was proposed that GMAP-210 recruits γ-tubulin to the Golgi, linking the Golgi to the centrosome and stabilizing the Golgi ribbon (Rios *et al.*, 2004). However, this hypothesis has been challenged with the discovery that the proposed γ-tubulin binding site corresponds to the GRAB domain (Gillingham *et al.*, 2004). A role for GMAP-210 in cilium formation has also been proposed. GMAP-210 anchors IFT20 to the Golgi, and mutation of GMAP-210 in mice and *Caenorhabditis elegans* results in a ciliogenesis defect (Follit *et al.*, 2008; Broekhuis *et al.*, 2013). More recently, mutations in human GMAP-210 were shown to cause the neonatal lethal skeletal dysplasia achondrogenesis type 1A (Smits *et al.*, 2010). The molecular mechanisms are not fully understood, but altered trafficking and Golgi fragmentation have been observed in GMAP-210–deficient fibroblasts and chondrocytes (Smits *et al.*, 2010). Thus there is conflicting evidence regarding the extent to which GMAP-210 participates in trafficking and Golgi organization in vivo. Moreover, the in vivo importance of the membrane-tethering function of GMAP-210, as opposed to its other potential roles in cells, has yet to be explored.

In this study, we show that tethering in vivo by GMAP-210 is mediated exclusively by the ALPS motif. GMAP-210 function in maintaining Golgi organization is dependent upon the ALPS-mediated tethering, indicating the functional importance of this process in vivo. Moreover, we show that binding to Rab2, although not required for tethering per se, is important for GMAP-210 functionality, most likely by coupling tethering with downstream processes important for Golgi integrity.

RESULTS

Knockdown of GMAP-210 causes disruption of the Golgi apparatus

To investigate GMAP-210 function in vivo, we depleted the protein using RNA interference (RNAi). We observed a dramatic compaction of the Golgi apparatus in GMAP-210–depleted cells compared with control cells (Figure 1, A and B). This effect was observed using four independent small interfering RNA (siRNA) oligonucleotides, which all effectively depleted the protein (Supplemental Figure S1, A and B). Of importance, Golgi morphology could be rescued by expression of siRNA-resistant GMAP-210 in the GMAP-210–depleted cells (Figure 1C; see also later discussion of Figure 4D), confirming the specificity of the phenotype. To determine whether the compaction of the Golgi apparatus was unique to this organelle or reflected a global change in cytoskeletal organization and organelle positioning, we performed double labeling with various markers. The positioning of early endosomes, lysosomes, and ER exit sites (ERESs) was unaffected by GMAP-210 depletion (Figure 1D). The gross organization of microtubules and F-actin was also not significantly altered in the GMAP-210–depleted cells (Supplemental Figure S2). Labeling with *cis*- and *trans*-Golgi markers indicated that, although highly condensed, the Golgi apparatus in GMAP-210–depleted cells retained its typical *cis*–*trans* polarity (Figure 1E).

Higher-resolution imaging using confocal microscopy indicated that the compact Golgi in GMAP-210–depleted cells appeared fragmented, comprising numerous distinct Golgi elements clustered close together (Figure 2A). To confirm the loss of Golgi ribbon continuity, we performed fluorescence recovery after photobleaching (FRAP). As shown in Figure 2, B and C, control cells stably expressing GalNAcT2–enhanced green fluorescent protein (GT2-GFP) showed rapid recovery after photobleaching, consistent with lateral linking of cisternae within the Golgi ribbon. In contrast, recovery was extremely poor in GMAP-210–depleted cells, reaching <20% of the starting fluorescence at 3 min of recovery (Figure 2, B and C). This result indicates that continuity between Golgi compartments is lost upon GMAP-210 depletion.

We next performed electron microscopy (EM) to analyze Golgi ultrastructure. In contrast to control cells, which had a typical stacked cisternal Golgi apparatus, there was a loss of Golgi stacks and cisternae, with a dramatic reduction in both cisternal number and length, upon GMAP-210 depletion (Figure 2, D and E). Instead, there was a striking accumulation of vesicular profiles of 50–70 nm in the Golgi region, together with larger vesicular profiles and vacuolar compartments that likely correspond to cisternal remnants (Figure 2, D and E). Of importance, the alterations in Golgi ultrastructure observed upon GMAP-210 depletion could be rescued by expression of siRNA-resistant GMAP-210, confirming specificity (see later discussion of Figure 5B). The accumulation of vesicular profiles is consistent with a loss of tethering at the Golgi apparatus, which would be expected to result in the accumulation of vesicles at the expense of cisternae.

GMAP-210 is required for assembly of the Golgi apparatus

We next wanted to investigate the role of GMAP-210 in Golgi biogenesis. For this purpose, we first treated cells with Golgicide A (GCA), a drug that specifically inhibits the Arf1 exchange factor GBF1, resulting in complete Golgi disassembly (Saenz *et al.*, 2009). Removal of GCA allows Golgi reformation, enabling us to investigate the requirement of GMAP-210 in this process. In both control and GMAP-210–depleted cells, the Golgi membrane protein golgin-84 was relocated to the ER within 2 h of GCA treatment (Supplemental Figure S3A, top). In control cells, the Golgi had re-formed its characteristic perinuclear ribbon organization at 90 min of washout, whereas it assumed a fragmented organization with numerous discrete structures adjacent to the nucleus in GMAP-210–depleted cells (Supplemental Figure S3A, middle). At 4 h of washout, typical elongated Golgi ribbons were seen in control cells, whereas the Golgi became highly compact, with a few remaining scattered elements, in GMAP-210–depleted cells (Supplemental Figure 3A, bottom). The reassembly defect was rescued by exogenous expression of siRNA-resistant GMAP-210 (Supplemental Figure S3B), indicating the phenotype was specific to GMAP-210 depletion. The defect in Golgi reassembly was also evident at the ultrastructural level. Clear Golgi stacks were observed in control cells at 90 min of GCA washout but were absent from the GMAP-210–depleted cells. Instead, there were numerous vacuolar and small vesicular profiles in the perinuclear region (Supplemental Figure S3C). These data indicate that GMAP-210 is required for Golgi assembly.

Mini-GMAP is unable to rescue GMAP-210 function in vivo

It was previously reported that a truncated GMAP-210, mini-GMAP, is sufficient to tether vesicles in vitro (Drin *et al.*, 2008). Mini-GMAP consists of the two membrane-interacting domains—the N-terminal

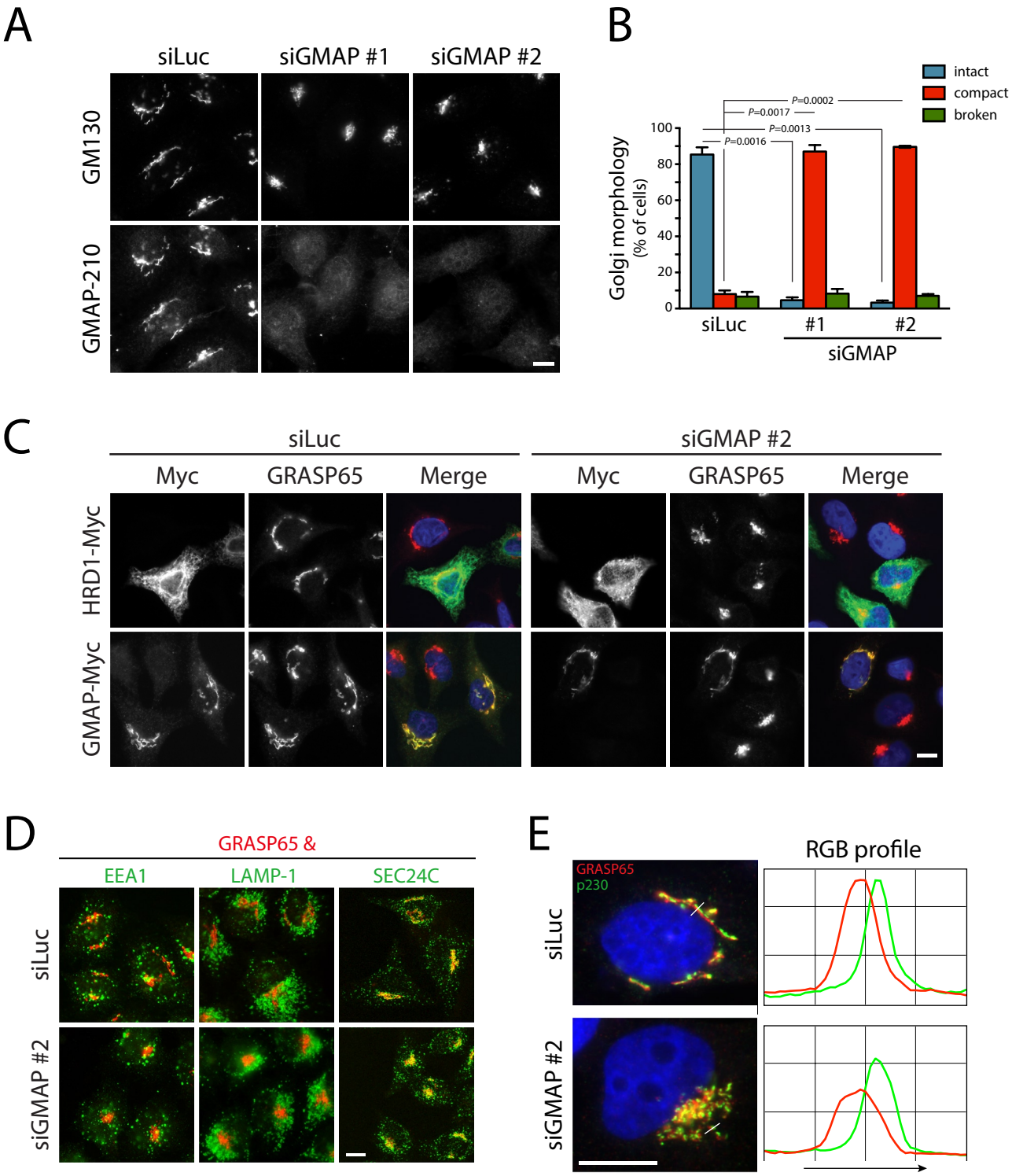

FIGURE 1: GMAP-210 is required for Golgi ribbon morphology. (A) HeLa cells transfected with control siRNA targeting luciferase (siLuc) or two independent siRNAs against GMAP-210 (siGMAP #1 and siGMAP #2) were labeled for endogenous GM130 and GMAP-210 and analyzed by fluorescence microscopy. (B) Percentage of cells displaying intact (thin and elongated), compact (short and condensed), and broken Golgi ribbon in control and GMAP-210–depleted cells ($n \geq 100$ cells/condition from three experiments). Error bars show SD, and p is determined by two-tailed Student's t test. (C) Luciferase- or GMAP-210–depleted HeLa cells were transfected with Myc-tagged HRD1 (control) or siRNA-resistant, Myc-tagged GMAP-210 and stained for Myc (green) and endogenous GRASP65 (red). (D) Merged images of siLuc- or siGMAP #2–treated HeLa cells double labeled for GRASP65 (red) and early endosome marker EEA1, lysosome marker LAMP-1, or ERES marker SEC24C (green). (E) Merged images of HeLa cells treated with siLuc or siGMAP #2 and labeled for GRASP65 (red) and p230 (green). White line indicates pixels used for RGB fluorescence intensity profile plots depicted on the right. Scale bars, 10 μm.

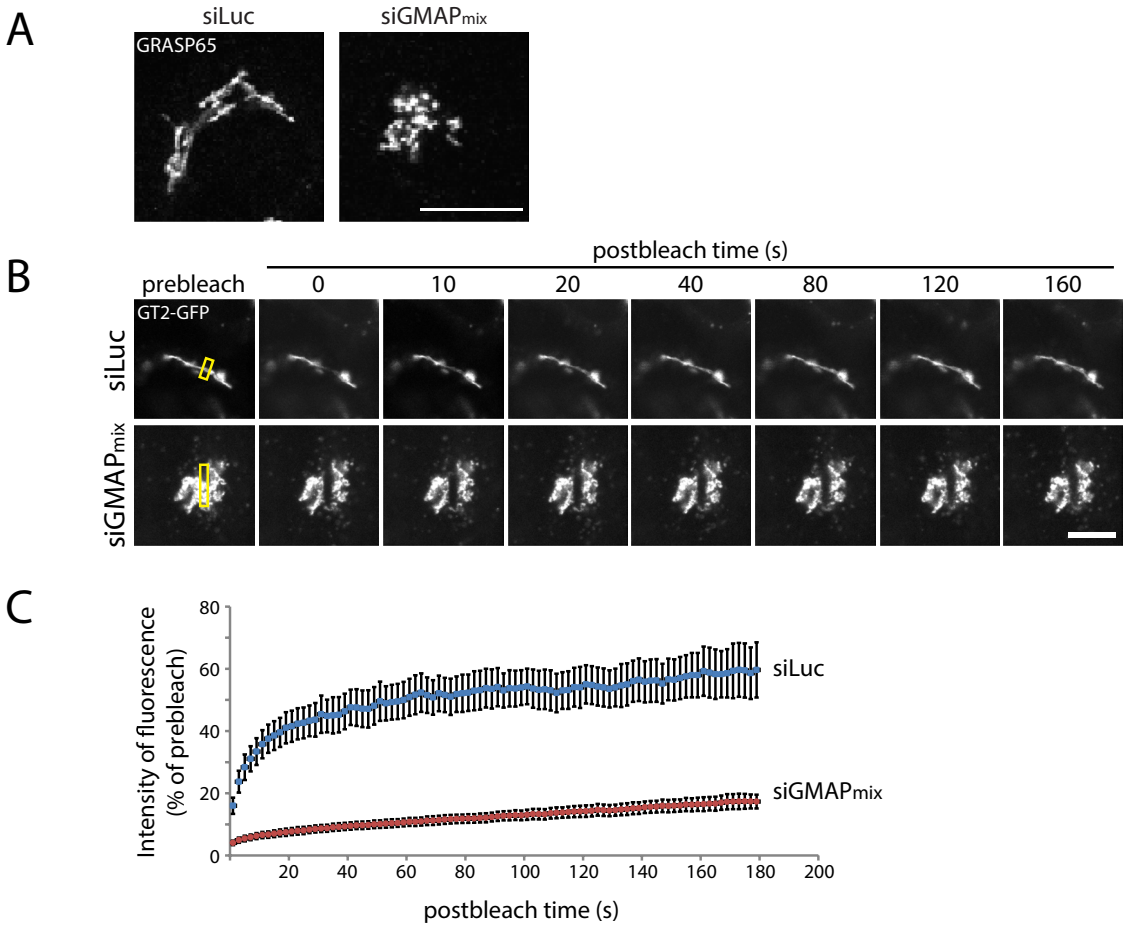

E

	siLuc	siGMAPmix
cisternae (no.)	6.9 ± 3.2	3.5 ± 2.6
cisternal remnants (no.)	2.7 ± 1.8	9.4 ± 3.9
vesicular profiles (no.)	34.9 ± 12.2	61.4 ± 20.5
cisternal length (nm)	790 ± 507 (84)	409 ± 167 (110)

FIGURE 2: Depletion of GMAP-210 vesiculates Golgi stacks. (A) Single focal plane from confocal laser microscopy images of the Golgi labeled for endogenous GRASP65 in control siLuc- or siGMAP-treated HeLa cells. A mixture of four individual siRNAs was used to knock down GMAP-210. (B) FRAP for the Golgi region (boxed in yellow) in HeLa cells stably expressing GT2-GFP was compared between control and GMAP-210–depleted cells. (C) Fluorescence in the bleached Golgi region from B as percentage of prebleach level (mean ± SD; $n = 19$ for siLuc and 28 for siGMAPmix). (D) Representative EM micrographs of control and GMAP-210–depleted HeLa cells. Cisternae are indicated by filled arrows, with cisternal remnants and vesicular profiles indicated by open arrows and filled arrowheads, respectively. (E) Table summarizing quantitation of membrane profiles (no.: number of profiles per unit of Golgi area) and cisternal

ALPS motif and the C-terminal GRAB domain—separated by a truncated coiled-coil that is approximately one-third that present in full-length GMAP-210 (predicted length of 90 vs. 260 nm for full-length GMAP-210, using 0.15 nm per amino acid of coiled-coil; Figure 3A). To determine whether mini-GMAP can fulfill GMAP-210's function in vivo, we performed RNAi rescue experiments and analyzed Golgi morphology. To our surprise, mini-GMAP was unable to rescue Golgi ribbon morphology (Figures 3A and 4D). Mini-GMAP was also unable to restore the stacked cisternal organization of the Golgi apparatus (see later discussion of Figure 6, D and E). These results indicate that the tethering ability of mini-GMAP is unable to rescue GMAP-210 function in vivo.

The coiled-coil region of GMAP-210 binds to Rab2

Possible explanations for the inability of mini-GMAP to rescue GMAP-210 function are that mini-GMAP is not long enough to function in vivo and that the central coiled-coil deleted in mini-GMAP interacts with additional factors important for in vivo functionality. We tested the latter possibility, since it was previously reported that the *Drosophila* homologue of GMAP-210 (dGMAP) can bind to Rab2 via its coiled-coil region, although the functional significance of Rab2 binding was not investigated in that study (Sinka *et al.*, 2008). We therefore investigated the ability of human GMAP-210 to interact with Rab proteins. Yeast two-hybrid analysis indicated that GMAP-210 specifically binds to Rab2 but not to the other Golgi-localized Rabs tested, namely Rab1, Rab6, and Rab33b, or to endosome-associated Rab5 (Figure 3B). Binding to Rab2 was confirmed using a glutathione *S*-transferase (GST) pull-down assay (Figure 3C). This assay further revealed that the interaction occurs only to the active, GTP-locked form of Rab2, as expected for an effector protein (Figure 3C). Next, we mapped the Rab2 binding site in GMAP-210 using the yeast two-hybrid assay and found that residues 1017–1195 and 1325–1599 within the coiled-coil region could bind to Rab2, with the first of these exhibiting stronger binding (Figure 3D). These two regions (1017–1195 and 1325–1599) are herein referred to as Rab2 binding domains 1 and 2 (RBD1 and RBD2), respectively. GST pull-down assays confirmed the interaction of RBD1 with the active form of Rab2 (Figure 3E). In comparison, Rab2 binding of a second fragment containing RBD2 was much weaker, although specific for the active form of Rab2 (Figure 3F). Deletion of regions within both RBD1 and RBD2 (ΔRBD; see Figure 4A) resulted in a complete loss of GMAP-210 binding to Rab2, indicating that no additional Rab2 binding sites are present in the protein (Figure 3G).

Rab2 binding domains of GMAP-210 are recruited to the Golgi in vivo

To determine whether the Rab binding domains of GMAP-210 are able to associate with Rab2 in vivo, we used a Golgi targeting assay. RBD1 was weakly targeted to the Golgi apparatus in control cells (Figure 3H). However, when endogenous GMAP-210 was depleted using RNAi, this fragment was efficiently recruited to the Golgi (Figure 3H). This result is consistent with Rab2-mediated recruitment to the Golgi membrane and also suggests that a significant proportion of Golgi-associated Rab2 is normally bound to GMAP-210. A fragment containing RBD2 also showed Golgi recruitment; however, the efficiency was lower than that for RBD1, consistent with weaker binding to Rab2 in vitro (Supplemental Figure S4). Neither of the Rab binding domains, although recruited to the Golgi, could rescue the compact Golgi phenotype (Figure 3H and Supplemental Figure S4).

The ALPS motif and Rab2 binding are required for the in vivo function of GMAP-210

We next wanted to investigate the requirement for the ALPS motif and Rab2 binding in GMAP-210 function in vivo. The ability to rescue the GMAP-210 depletion phenotype in cells allowed us to dissect the relative importance of these two potential tethering mechanisms in vivo. For this purpose, we generated various deletion constructs that lacked either the ALPS motif or the Rab2 binding site alone or lacked both domains (Figure 4A). We also generated a construct additionally lacking the C-terminal GRAB domain, which is important for anchoring the C-terminus of GMAP-210 to cisternal membranes (Figure 4A).

In addition to determining the ability of each construct to rescue Golgi morphology, we analyzed their targeting to Golgi membranes. Performing this experiment in GMAP-210–depleted cells avoided complications arising from dimerization of the deletion constructs with the endogenous protein. Deletion of the ALPS motif or the Rab2 binding site alone or both domains in combination did not affect Golgi recruitment of GMAP-210 (Figure 4B). This was most likely due to targeting by the C-terminal GRAB domain, since deletion of the C-terminus in addition to the ALPS motif and Rab2 binding site completely abolished Golgi localization (Figure 4B). We also analyzed the ability of the deletion constructs to target to the ER-GIC, to which GMAP-210 is recruited upon treatment of cells with brefeldin-A (BFA; Rios *et al.*, 1994). As expected, full-length GMAP-210 was localized to the ERGIC when expressed in BFA-treated cells depleted of endogenous GMAP-210 (Figure 4C). Targeting to the ERGIC still occurred upon deletion of the ALPS or Rab2 binding domains alone or together. Additional deletion of the C-terminus resulted in complete dispersal of GMAP-210, indicating a contribution to ERGIC recruitment under these conditions. This effect is likely due to a C-terminal determinant other than the GRAB domain because Arf1 will be absent from the membranes after BFA treatment, with the short amphipathic helix found adjacent to the GRAB domain a good candidate (Gillingham *et al.*, 2004; Drin *et al.*, 2008). The results indicate that the C-terminus of GMAP-210 is important for recruitment to both the Golgi and ERGIC.

To monitor the ability of different GMAP-210 constructs to restore Golgi structure using the RNAi rescue approach, we analyzed only cells expressing moderate levels of GMAP-210 protein, as judged by fluorescence intensity. This was important because high-level overexpression of GMAP-210 has been reported to fragment the Golgi apparatus (Infante *et al.*, 1999; Pernet-Gallay *et al.*, 2002; Friggi-Grelin *et al.*, 2006). Expression of full-length GMAP-210 in the GMAP-210–depleted cells efficiently rescued Golgi ribbon morphology, as described earlier (Figures 1C and 4, B and D). Surprisingly, expression of the ΔALPS mutant also rescued Golgi morphology, albeit to a lesser extent than the full-length protein; this effect was most obviously indicated by the "long plus short ribbon" category (Figure 4, B and D). Deletion of the Rab2 binding site (ΔRBD) had a stronger effect upon rescue efficiency. Compared to the ΔALPS construct, there were significantly fewer cells with a "long" Golgi ribbon and significantly more with a compact Golgi phenotype in the ΔRBD

length (in nanometers). The parameters were determined as described *Materials and Methods*, and results are expressed as mean ± SD ($n = 15$ for siLuc and 25 for siGMAPmix, where n is the number of Golgi fields counted). Numbers in parenthesis indicate number of Golgi cisternae for which the length was measured. All analyses passed the Student's t test ($p < 0.05$). Scale bars, 10 μm (A, B), 0.5 μm (D).

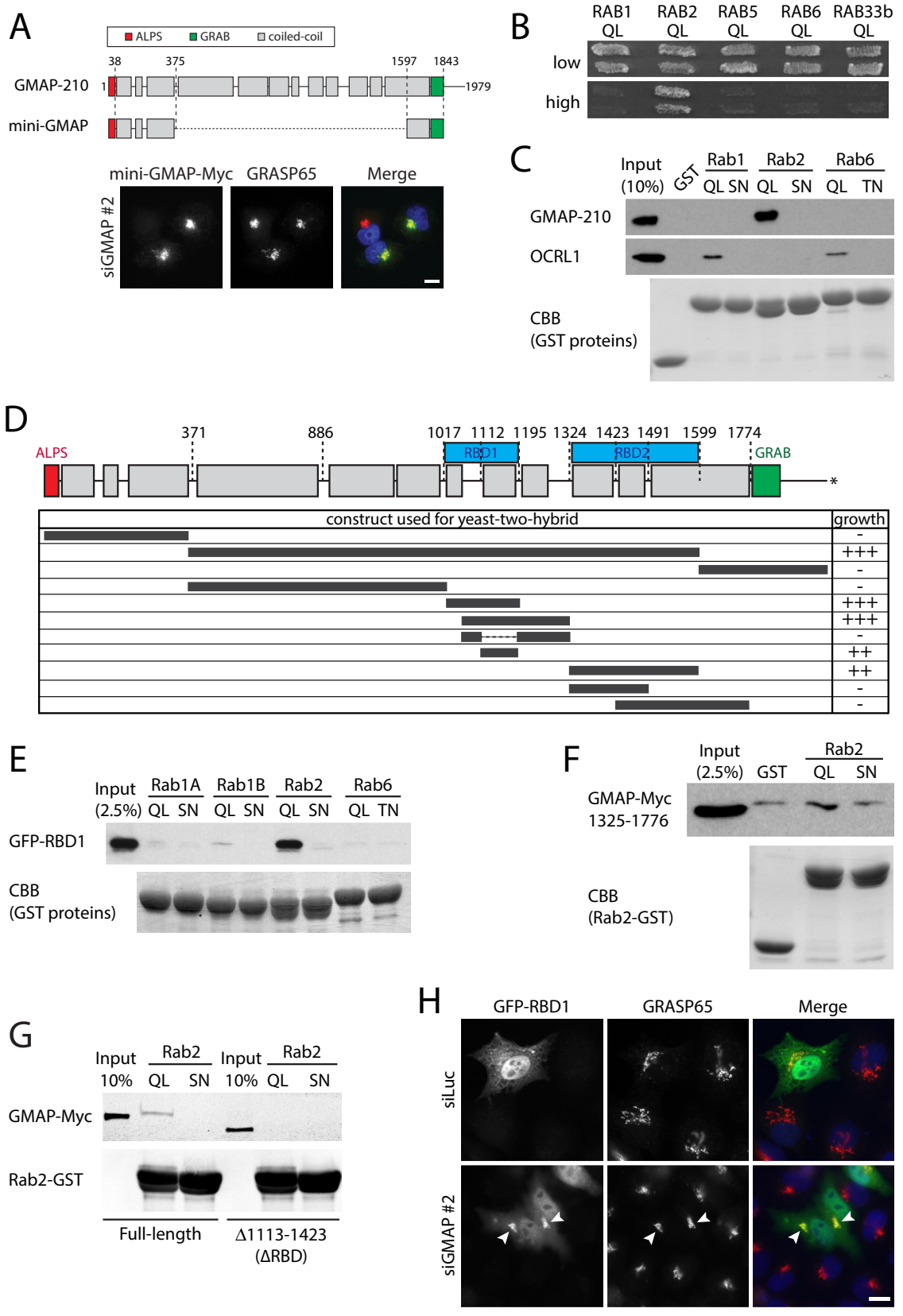

FIGURE 3: GMAP-210 interacts with Rab2 in its central region. (A) Domain organization of GMAP-210 and schematic representation of the mini-GMAP construct. GMAP-210–depleted HeLa cells expressing mini-GMAP-Myc were stained for the Myc epitope (green) and endogenous GRASP65 (red). (B) Full-length GMAP-210 was tested for interaction in the yeast two-hybrid system with constitutively active mutants of Rab proteins (Rab1 Q70L, Rab2 Q65L, Rab5 Q79L, Rab6 Q72L, and Rab33b Q92L). (C) HeLa cell extracts were incubated with GST or GST-tagged Rab proteins carrying constitutively active (Rab1 Q70L, Rab2 Q65L, Rab6 Q72L) or dominant-negative (Rab1 S25N, Rab2 S20N, Rab6 T27N)

mutant (Figure 4, B and D). Deletion of both the ALPS motif and the Rab2 binding site almost completely abolished the ability to rescue (Figure 4, B and D). Therefore both domains function in Golgi ribbon formation. Additional deletion of the GRAB domain in the Δ(ALPS+RBD+CT) mutant also failed to rescue Golgi morphology, as expected (Figure 4, B and D).

We next monitored Golgi ultrastructure in the RNAi rescue experiments. For this purpose we used correlative light-electron microscopy (CLEM), which allows EM analysis of cells first identified by fluorescence microscopy. Expression of full-length GMAP-210 was able to restore formation of stacked Golgi cisternae in the depleted cells (Figure 5, A and B). Deletion of the ALPS motif from full-length GMAP-210 significantly impaired rescue of Golgi ultrastructure. There was some restoration of cisternae, although they were much shorter than those seen with wild-type GMAP-210, and there was a near-complete loss of vacuolar cisternal remnants (Figure 5, A and B). Vesicles were particularly abundant upon rescue with the ΔALPS mutant, consistent with a defect in vesicle tethering in these cells (Figure 5, A and B). Loss of Rab2 binding also impaired rescue of Golgi ultrastructure, indicated by the presence of cisternae, which again were much shorter than with wild-type GMAP-210, and a lack of vacuolar remnants (Figure 5, A and B). There were also numerous vesicles, albeit fewer than with the ΔALPS mutant (Figure 5, A and B). Deletion of both the ALPS motif and Rab2 binding site severely impaired the rescue of Golgi morphology (Figure 5, A and B). There were reduced numbers of short Golgi cisternae and numerous vesicles and cisternal remnants. The ability of both the ALPS motif and the Rab2 binding site to contribute to the formation of cisternae from vesicles indicates a functional role for both domains in vivo.

GMAP-210 length is important for its in vivo function

To investigate the extent to which the failure of mini-GMAP to rescue Golgi morphology was due to loss of the central Rab2 binding domain or to its decreased length, we engineered a construct in which RBD1, the predominant Rab2 binding site, was reintroduced into mini-GMAP (Figure 6A). This construct was able to bind Rab2 as efficiently as the full-length protein, whereas mini-GMAP was unable to bind, as expected (Figure 6B). However, it was unable to restore Golgi ribbon organization in GMAP-210–depleted cells (Figure 6C). The compact Golgi phenotype was no longer observed, but instead of forming a typical Golgi ribbon, the Golgi assumed a dispersed, broken-ribbon phenotype (Figure 6C). Thus gaining Rab2 binding led to dispersal of the compact Golgi but not the completion of ribbon formation. At the ultrastructural level, Golgi membranes appeared in discrete clusters, consistent with the dispersed nature of the staining seen by light microscopy (Figure 6D). Although there was some restoration of cisternae compared with mini-GMAP, they were shorter than those obtained with full-length GMAP-210, and there was an abundance of vesicular profiles (Figure 6, D and E). Hence inclusion of the Rab2 binding site in mini-GMAP is unable to restore Golgi ultrastructure. The results suggest that loss of Rab2 binding is not the sole reason for the failure of mini-GMAP to rescue Golgi organization. Instead, they suggest that the length of the protein is also important for GMAP-210 to fulfill its function in vivo.

GMAP-210 can tether Golgi vesicles in vivo

It was previously shown that mini-GMAP can tether vesicles in vitro (Drin *et al.*, 2008), and a recent study using mitochondrial targeting of full-length GMAP-210 showed that it is competent to tether Golgi-derived vesicles within the cell (Wong and Munro, 2014). Although the ALPS motif, Rab2 binding, and length are all required for GMAP-210 function at the Golgi apparatus, how they contribute to function is unclear. We may envisage that the ALPS motif and Rab2 binding both contribute to vesicle tethering, but is this true? To answer this question, we took advantage of the in vivo vesicle-tethering assay devised by Wong and Munro (2014). We first confirmed that GMAP-210 was able to tether Golgi-derived vesicles. For this purpose, we replaced the C-terminal region of GMAP-210 containing the GRAB domain with FKBP and coexpressed the protein in cells with mitochondrially localized FRB, which allowed mitochondrial targeting of GMAP-210 upon addition of rapamycin (Figure 7A). As shown in Figure 7B, in the absence of rapamycin, GMAP-210-Myc-FKBP12 was present at the Golgi apparatus; this was due to the ALPS motif and Rab2 binding, since deletion of both determinants resulted in a cytosolic distribution (Figure 8). On addition of rapamycin, GMAP-210-Myc-FKBP12 was relocated to mitochondria (Figure 7B). As observed previously (Wong and Munro, 2014), there was accumulation of the Golgi-resident enzyme GalNAcT2 at the GMAP-210–positive mitochondria, consistent with tethering of Golgi-derived vesicles (Figure 7B; see also later discussion of Figure 9). This could be better visualized upon treatment of cells with nocodazole to disperse the Golgi apparatus (Figure 7B; see also later discussion of Figure 9). There was also tethering of golgin-84–containing vesicles, whereas the TGN residents TGN46 and GORAB were not tethered, consistent with tethering of Golgi stack–derived vesicles but not those derived from the TGN (Figure 7B and Supplemental Figure S5; see also later discussion of Figure 9). The Golgi was fragmented upon GMAP-210 relocation to mitochondria (Figure 7B and Supplemental Figure S5; see also later discussion of Figure 9), most likely due to mistargeting to and accumulation of Golgi-derived vesicles at mitochondria instead of their correct delivery to the Golgi apparatus.

Vesicle tethering by GMAP-210 requires the ALPS motif but not Rab2 binding

Having confirmed that GMAP-210 can tether Golgi vesicles in vivo, we next tested the requirements for tethering. Removal of both the ALPS motif and the Rab2 binding site completely abrogated tethering of GalNAcT2 and golgin-84–containing vesicles (Figure 8; see also Figure 9 and Supplemental Figure S5). These results indicate that GMAP-210 lacks additional vesicle tethering determinants. The lack of tethering also indicates that heterodimerization of mitochondrially targeted GMAP-210 with the endogenous protein, although formally possible, does not result in significant tethering in the assay. Strikingly, removal of the ALPS motif alone completely

mutations and bound proteins analyzed by Western blotting with the indicated antibodies. GST-Rab proteins on beads were analyzed by Coomassie brilliant blue (CBB) staining. (D) The indicated GMAP-210 fragments were tested for interaction with the constitutively active Rab2 Q65L mutant in the yeast two-hybrid system. (E–G) HEK293 cells expressing GFP-RBD1 (E), GMAP-Myc residues 1325–1776 (F), or full-length GMAP-210-Myc or GMAP-210-Myc lacking residues 1113–1423 (ΔRBD; G) were incubated with the indicated constitutively active or inactive GST-tagged Rabs and binding assessed by Western blotting. Equal loading of beads with GST or GST-Rabs was determined by CBB staining (E, F) or Western blotting with anti-GST (G). (H) HeLa cells treated with siLuc or siGMAP #2 were transfected with GFP-RBD1 and stained for endogenous GRASP65. Arrowheads indicate targeting of GFP-RBD1 to the Golgi apparatus. Scale bars, 10 μm.

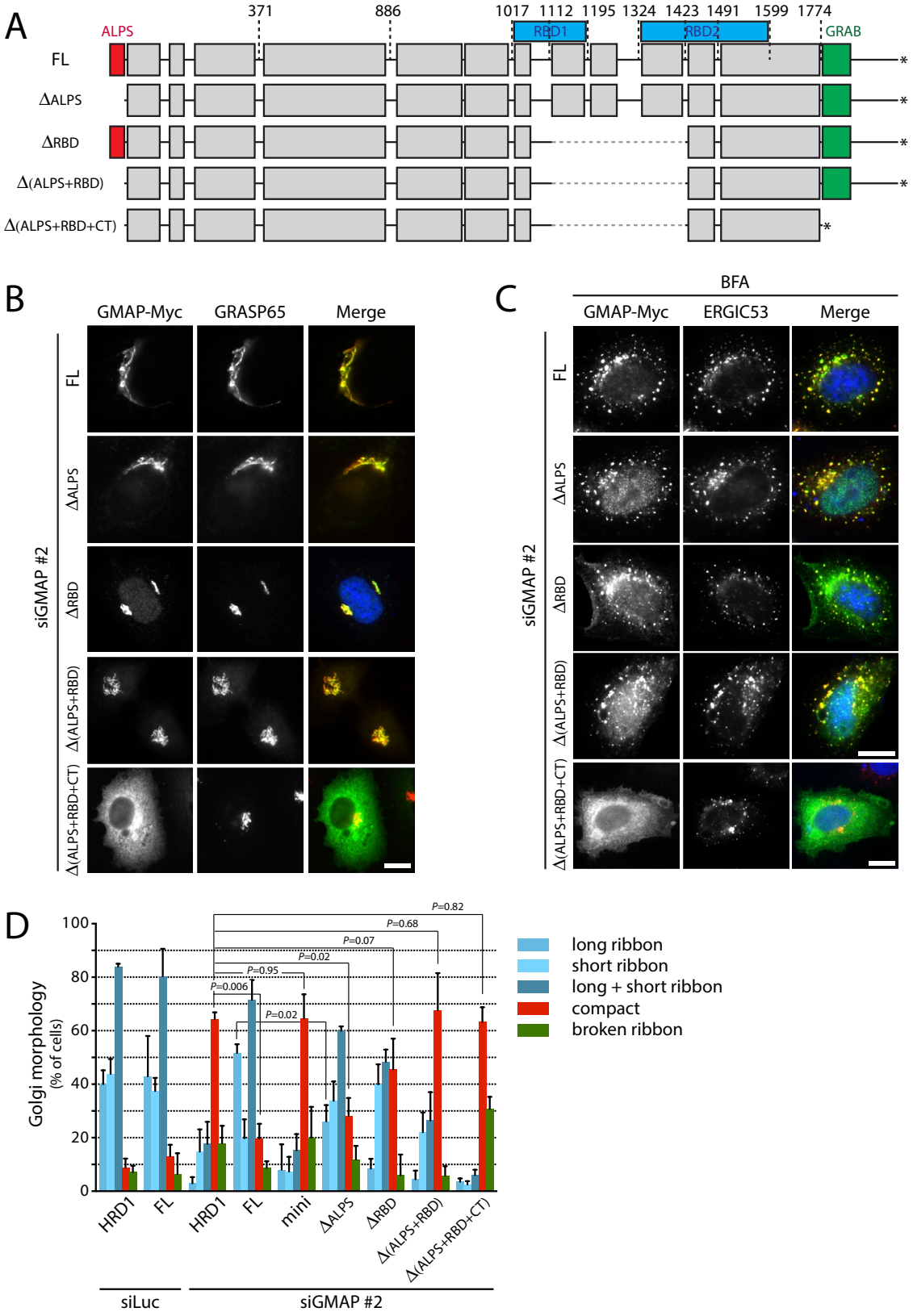

FIGURE 4: Domain requirements for the in vivo function of GMAP-210. (A) Schematic representation of the Myc-tagged GMAP-210 truncated mutants used for the Golgi ribbon rescue analysis. (B, C) HeLa cells treated with siGMAP #2 were transfected with full-length GMAP-210-Myc or the indicated truncated mutants and either left untreated (B) or treated with 5 μg/ml BFA for 1 h (C) before staining for the Myc epitope (green) and endogenous GRASP65 (red). Scale bars, 10 μm. (D) Quantitation of the Golgi phenotype from B and Figure 3A. HRD1 indicates cells transfected with HRD1-Myc as a control. The percentage of cells displaying long (at least half the length of the nuclear diameter),

A

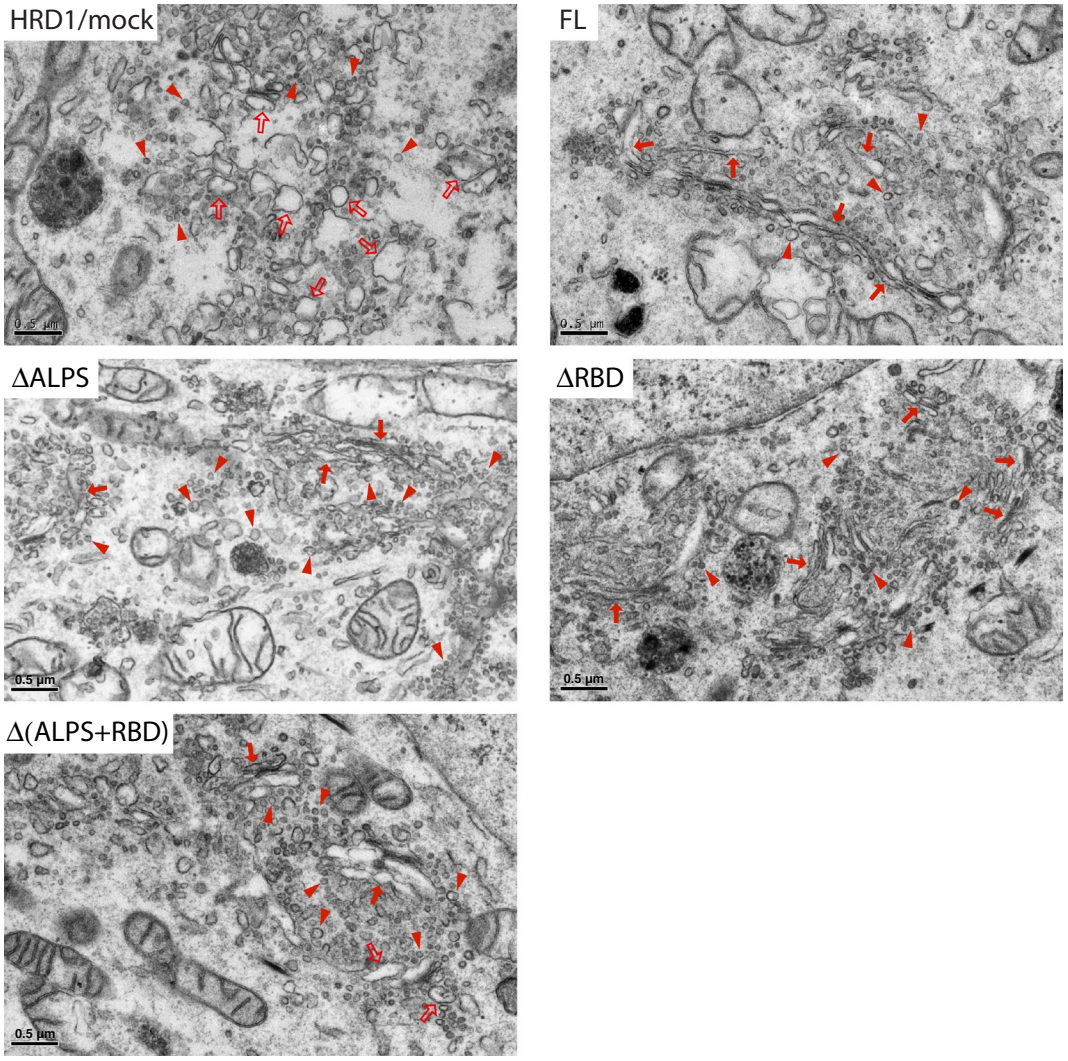

B

	siGMAP #2				
Rescue	HRD1/mock	FL	ΔALPS	ΔRBD	Δ(ALPS+RBD)
cisternae (no.)	1.1 ± 1.3	6.4 ± 2.1	8.8 ± 2.0	6.6 ± 1.6	3.6 ± 1.6
cisternal remnants (no.)	12.2 ± 3.1	2.5 ± 1.9	3.2 ± 2.0	2.4 ± 1.4	4.2 ± 3.2
vesicular profiles (no.)	53.6 ± 8.1	35.7 ± 9.9	90.8 ± 24.9	61.6 ± 14.6	61.9 ± 15.8
cisternal length (nm)	350 ± 138 (67)	781 ± 467 (208)	422 ± 237 (232)	500 ± 238 (160)	463 ± 192 (195)

FIGURE 5: Expression of GMAP-210 rescue constructs differentially restores Golgi ultrastructure. (A) HeLa cells depleted of GMAP-210 using siGMAP #2 duplex were transfected with HRD1-Myc as a control or siRNA-resistant, full-length GMAP-210-Myc or the indicated deletion mutants. Cells were stained for the Myc epitope and endogenous GRASP65 and analyzed by fluorescence microscopy before examination of representative cells (Figure 4, B and D) by EM. Golgi cisternae (closed arrows), cisternal remnants (open arrows), and vesicles (arrowheads) are indicated. Scale bars, 0.5 µm. (B) Table summarizing the results from the rescue experiments in A. Values are mean ± SD (HRD1/mock, $n = 15$; full length, $n = 13$; ΔALPS, $n = 12$; ΔRBD, $n = 10$; Δ(ALPS+RBD), $n = 11$; where n is the number of Golgi fields counted). Shown are number of profiles per unit Golgi area (no.) and cisternal length (in nanometers). Numbers in parenthesis indicate the number of Golgi cisternae for which the length was measured.

short (less than half the length of the nuclear diameter), compact (thick and condensed), or broken Golgi ribbon was determined ($n > 100$ cells per condition from three experiments). Error bars show SD; p is determined by a two-tailed Student's t test.

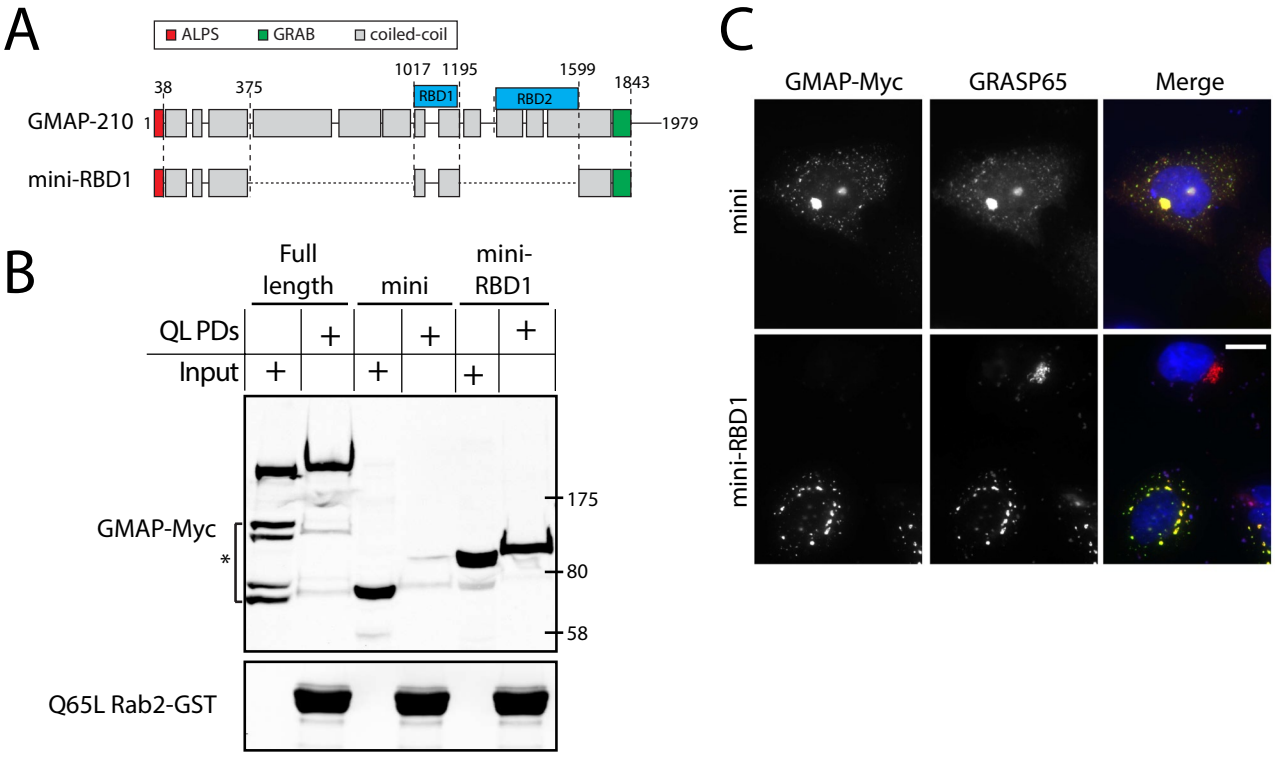

E

	siGMAP #2			
Rescue	HRD1/mock	FL	mini	mini-RBD1
cisternae (no.)	1.1 ± 1.3	6.4 ± 2.1	3.5 ± 2.3	6.2 ± 2.9
cisternal remnants (no.)	12.2 ± 3.1	2.5 ± 1.9	9.2 ± 2.1	6.1 ± 3.1
vesicular profiles (no.)	53.6 ± 8.1	35.7 ± 9.9	68.5 ± 11.6	95.8 ± 11.4
cisternal length (nm)	350 ± 138 (67)	781 ± 467 (208)	470 ± 214 (156)	408 ± 209 (241)

FIGURE 6: Rab2 binding cannot restore functionality to mini-GMAP in Golgi organization. (A) Schematic representation of the mini-GMAP-RBD1 construct. (B) Lysates of HEK293 cells expressing full-length GMAP-210-Myc, mini-GMAP-Myc, or mini-GMAP-RBD1-Myc were incubated with the constitutively active Q69L Rab2 and binding monitored by Western blotting with anti-Myc antibody. The asterisk indicates degradation products of full-length GMAP-210-Myc. (C) HeLa cells treated with siGMAP #2 were transfected with mini-GMAP-Myc or mini-GMAP-RBD1-Myc and stained for the Myc epitope (green) and endogenous GRASP65 (red). Scale bar, 10 µm. (D) CLEM analysis of cells rescued by expression of mini-GMAP or mini-GMAP-RBD1. Golgi cisternae (closed arrows), cisternal remnants (open arrows), and vesicles (arrowheads) are indicated. Scale bars, 0.5 µm. (E) Table summarizing the results from the rescue experiments

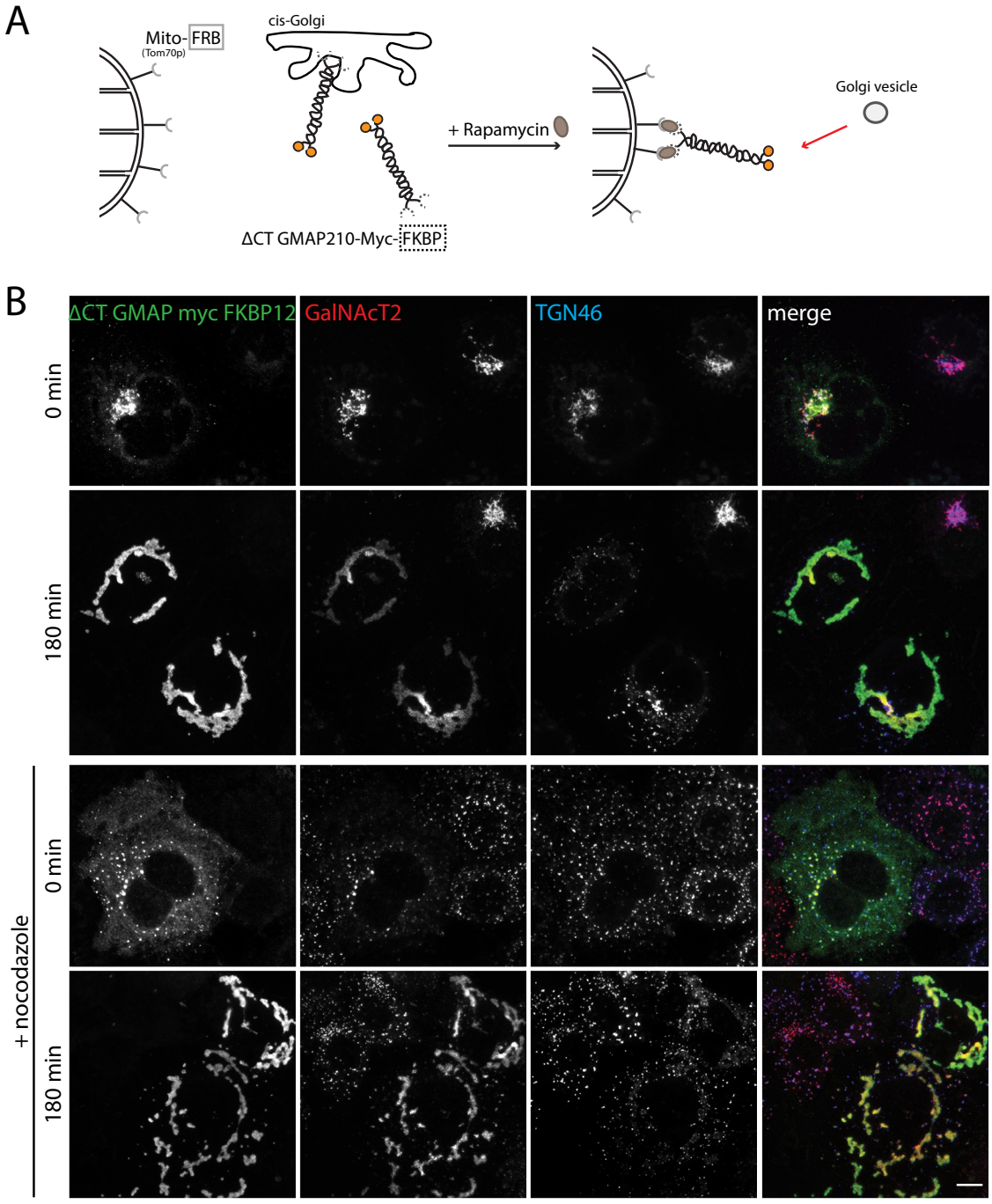

FIGURE 7: Reroutable GMAP-210 relocates the Golgi enzyme GalNAcT2, but not TGN46, to mitochondria. (A) Schematic of relocation of GMAP-210 to mitochondria for the vesicle-tethering assay; design of ΔCT GMAP210-Myc fused to FKBP (dotted line) and Mito (Tom70p) fused to FRB (gray line). ΔCT GMAP210-Myc-FKBP is rapidly relocated from Golgi to mitochondria upon rapamycin-induced heterodimerization of the FKBP and FRB domains. (B) COS7 cells coexpressing ΔCT GMAP-210-Myc-FKBP along with Mito-FRB were left untreated or treated with nocodazole for 2 h before induction of mitochondrial relocation with rapamycin for a further 3 h. Cells were costained for the Myc epitope (green) to detect the reroutable GMAP-210, the Golgi enzyme, GalNAcT2 (red), and the *trans*-Golgi and TGN-resident protein TGN46 (blue). Scale bar, 10 μm.

in D. Values are mean ± SD (mini, $n = 11$; mini-RBD1, $n = 10$; where n is the number of Golgi fields counted). Shown are number of profiles per unit Golgi area (no.) and cisternal length (in nanometers). Numbers in parenthesis indicate the number of Golgi cisternae for which the length was measured. Note that the numbers for HRD1/mock and full length are the same as those used in Figure 5B; the experiments were done together, but the data are separated for clearer presentation.

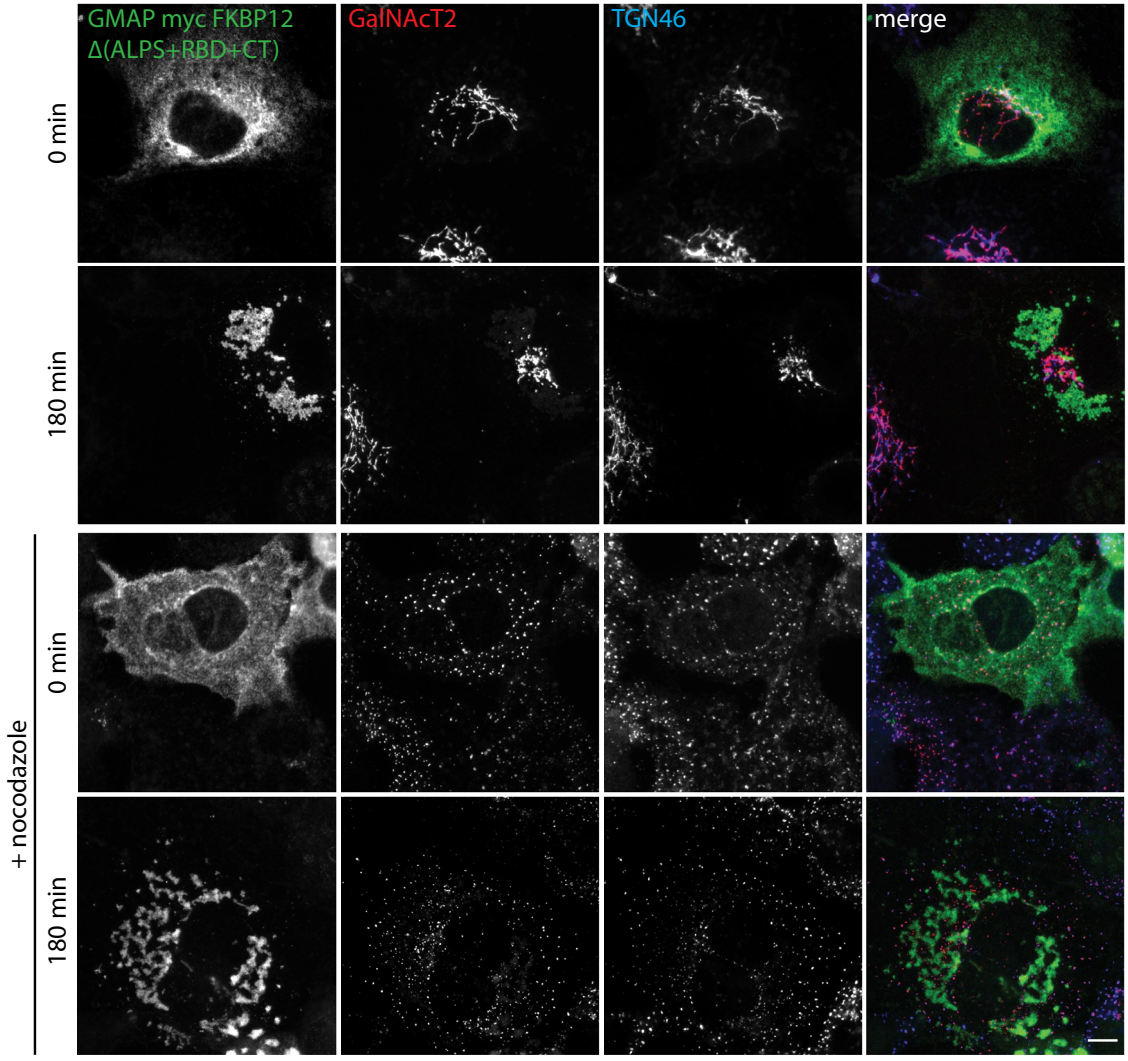

FIGURE 8: Removal of the ALPS and Rab2-binding domains abolishes tethering of GalNAcT2 by GMAP-210. COS7 cells coexpressing Δ(ALPS+RBD+CT) GMAP-210-Myc-FKBP along with Mito-FRB were left untreated or treated with nocodazole for 2 h before induction of mitochondrial relocation with rapamycin for a further 3 h. Cells were costained for the Myc epitope (green), GalNAcT2 (red), and the *trans*-Golgi marker TGN46 (blue). Scale bar, 10 μm.

abolished tethering, whereas deletion of the Rab2 binding site had no effect (Figure 9 and Supplemental Figure S5), indicating that the ALPS motif is the major vesicle-tethering determinant in GMAP-210 and that Rab2 binding is dispensable for tethering.

GMAP-210 length is not required for vesicle tethering with the Golgi

We next investigated whether length of GMAP-210 was important for vesicle tethering at mitochondria. As shown in Figure 9 and Supplemental Figure S5, mini-GMAP could tether vesicles at mitochondria as efficiently as GMAP-210 lacking only the C-terminus. Inclusion of the Rab2 binding site in mini-GMAP had no effect on tethering, consistent with the lack of Rab2 involvement in the vesicle-tethering reaction (Figure 9 and Supplemental Figure S5). Thus, although mini-GMAP is functionally deficient at the Golgi apparatus, it is fully competent to tether Golgi vesicles to mitochondria.

DISCUSSION

Golgins have been proposed to function as membrane tethers that link transport vesicles to Golgi cisternae or connect cisternal or tubulovesicular Golgi elements for maintenance of Golgi structure (Ramirez and Lowe, 2009; Munro, 2011). In most cases, tethering is likely followed by membrane fusion, although one could also envisage stable golgin-mediated cross-links, as has been proposed for cisternal stacking (Lee *et al.*, 2014). The extended conformation of golgins combined with their anchoring to Golgi membranes at one end makes them attractive candidates for Golgi tethers. However, until recently, in vivo evidence for golgin-mediated tethering has been lacking. Our results indicate that GMAP-210 can function as a Golgi vesicle tether in vivo. This observation is in accordance with the findings of Wong and Munro (2014), who provided the first evidence that different golgins, including GMAP-210, are competent to tether transport vesicles in vivo. Thus it appears that most golgins are indeed membrane tethers.

Despite this important advance, the mechanisms underlying golgin-mediated tethering, as well as how tethering is linked to downstream membrane fusion events, remain poorly defined. We show here that GMAP-210–mediated tethering in cells is mediated exclusively by the N-terminal ALPS motif. On the face of it, this may appear surprising. Tethering is a specific process, with different golgins able to tether different types of vesicles (Wong and Munro, 2014), yet the ALPS motif binds to membrane

lipids (Drin *et al.*, 2007, 2008). However, it has been demonstrated that the ALPS motif, despite binding lipids, can selectively recognize vesicles in the early secretory pathway (Pranke *et al.*, 2011). The ALPS motif can therefore tether vesicles in a specific manner.

The ALPS motif is not present in other golgins, suggesting that they tether vesicles through other determinants. GM130 and giantin bind the vesicle docking protein p115 at their extreme N-termini, and these interactions have been proposed to tether vesicles (Nakamura *et al.*, 1997). Although the situation for other golgins is less clear, it is tempting to speculate that they also mediate tethering through determinants present at their extreme N-termini. This would be expected to increase the efficiency of vesicle tethering by increasing accessibility at the Golgi membrane surface (see also later discussion), as well as increasing the radius of capture. Of interest, the ALPS motif is poorly conserved in nonvertebrates. Either GMAP-210 orthologues in these species are not primarily vesicle tethers or tethering is mediated through a different mechanism. Further work will be required to distinguish between these possibilities.

Although most golgins bind to Rab GTPases through their coiled-coil regions (Sinka *et al.*, 2008; Hayes *et al.*, 2009; Munro, 2011), the significance of Rab binding has until now been unclear. We show here that Rab2 binding is dispensable for tethering, although it is required for GMAP-210 functionality at the Golgi apparatus. This strongly suggests that Rab2 binding occurs downstream from vesicle tethering. A working model is presented in Figure 10. Initial capture of a vesicle is mediated by the ALPS motif. Vesicle-associated Rab2 then mediates attachment to the Rab2 binding site within the central coiled-coil region of GMAP-210, bringing the vesicle into closer proximity to the target membrane. This promotes engagement of soluble *N*-ethylmaleimide–sensitive factor attachment protein receptors (SNAREs), which occurs over a short distance, leading ultimately to fusion. This model is in agreement with studies showing that Rab and SNARE machineries act coordinately to promote membrane fusion (Haas *et al.*, 1995; Allan *et al.*, 2000; Ohya *et al.*, 2009). The presence of two vesicle attachment sites on GMAP-210 would allow the vesicle to "hop" along GMAP-210, as has been suggested (Ramirez and Lowe, 2009). Of course, the vesicle could also hop onto adjacent golgins if these too contain Rab2 binding sites, whereas Rab2-containing vesicles tethered by other golgins could hop onto GMAP-210, as implied in the tentacle model (Sinka *et al.*, 2008). This phenomenon could explain the partial functionality of the ΔALPS and Rab2 binding mutants in rescuing Golgi structure. The presence of two vesicle attachment sites in GMAP-210 (ALPS motif and Rab2 binding site) would also be expected to improve the fidelity of trafficking, providing distinct proofreading steps before the downstream membrane fusion reaction. The Golgi matrix, which comprises a network of golgins with multiple Rab binding sites, could therefore act as a selectivity filter to ensure tethered vesicles progress to the correct Golgi subcompartment before fusion occurs (Munro, 2011).

Golgins are in part defined by their high content of coiled-coil, resulting in a predicted extended conformation. As mentioned, this would be expected to improve efficiency of vesicle capture (Ramirez and Lowe, 2009; Munro, 2011). The inability of mini-GMAP, either with or without the Rab2 binding site, to rescue GMAP-210 depletion would fit with such a view. Surprisingly, however, mini-GMAP functioned as an efficient vesicle tether when targeted to mitochondria. Thus length is not critical for in vivo vesicle tethering per se, as was also shown in vitro (Drin *et al.*, 2008). Why, then, can mini-GMAP not rescue Golgi structure? An important distinction between the Golgi apparatus and mitochondria is the presence of the Golgi matrix, which is believed to surround the organelle in a dense, mesh-like network (Lowe, 2011). For the ALPS motif to be recognized by transport vesicles, it needs to be accessible. The extended conformation of GMAP-210 allows for this, whereas in mini-GMAP, which is noticeably shorter (90 vs. 260 nm), the ALPS motif is likely buried in the matrix and inaccessible to transport vesicles. The Golgi matrix model described here would also be consistent with golgins using extreme N-terminal determinants for vesicle tethering. Rab binding sites, which reside within the central coiled-coil regions of golgins, are less likely to be exposed on the surface of the Golgi matrix and are more likely to function downstream to couple tethering with fusion.

Two previous studies failed to observe Golgi vesiculation upon depletion of GMAP-210 by RNAi. In both studies, performed with the same siRNA, the Golgi ribbon was fragmented but stacked cisternal organization was maintained (Rios *et al.*, 2004; Yadav *et al.*, 2009). The reasons for the differences in phenotype between these studies and ours, in which we observe clear and dramatic Golgi vesiculation, are unclear. A trivial explanation is that they may be attributable to differences in depletion efficiency. Nonetheless, we are confident that our phenotype is specific; it was seen with four independent siRNAs and could be rescued by reexpression of nonsilenced GMAP-210. It should also be noted that in certain cell types of the GMAP-210–knockout mouse, the Golgi is highly vesiculated, phenocopying what we report in this study (Smits *et al.*, 2010).

A striking feature of GMAP-210 depletion is Golgi compaction. This could simply reflect a loss of Golgi organization at the ultrastructural level, resulting in a reduced volume of cytoplasm occupied by the disrupted Golgi membranes. Alternatively, it could indicate a defect in microtubule organization or in the way that the Golgi associates with microtubules (Chabin-Brion *et al.*, 2001; Rios *et al.*, 2004). The former seems unlikely, since the microtubule cytoskeleton appears normal in GMAP-210–depleted cells, although we cannot exclude a subtle change in microtubule organization or dynamics. Reduced nucleation of microtubules at the Golgi apparatus, which is important for ribbon extension, could in principle explain the compact Golgi phenotype (Miller *et al.*, 2009; Hurtado *et al.*, 2011). In this case, centrosomally nucleated microtubules would dominate, pulling the Golgi membranes closer to the centrosome, thereby causing compaction. GMAP-210 was previously shown to bind γ-tubulin (Rios *et al.*, 2004), so a role in Golgi nucleation is plausible, although a subsequent study failed to observe any defect in microtubule nucleation at the Golgi in GMAP-210–depleted cells (Rivero *et al.*, 2009). Further studies will be required to determine the precise mechanisms causing Golgi compaction upon GMAP-210 depletion.

MATERIALS AND METHODS

Reagents and antibodies

All reagents were from Sigma-Aldrich (Poole, United Kingdom) or Merck Chemicals (Nottingham, United Kingdom), unless stated otherwise. Sheep polyclonal anti–GMAP-210 was raised against maltose-binding protein fused to amino acids 1–375 of human GMAP-210. Mouse monoclonal antibodies against GMAP-210, EEA1, and p230 were obtained from BD Biosciences (Oxford, United Kingdom). Rabbit polyclonal anti-GMAP-210 was a generous gift from Francis Barr (University of Oxford, Oxford, United Kingdom). Mouse monoclonal anti-Myc antibodies, clones 9E10 and 9B11, were from Sigma-Aldrich and Cell Signaling Technology (Danvers, MA) respectively, and rabbit polyclonal anti-Myc was from Abcam (Cambridge, United Kingdom). Mouse monoclonal anti-ERGIC53 was from Enzo Life Sciences (Exeter, United Kingdom). Mouse monoclonal anti–LAMP-1 was obtained from the Developmental Studies Hybridoma Bank (University of Iowa, Iowa City, IA). Mouse monoclonal anti-GalNAcT2

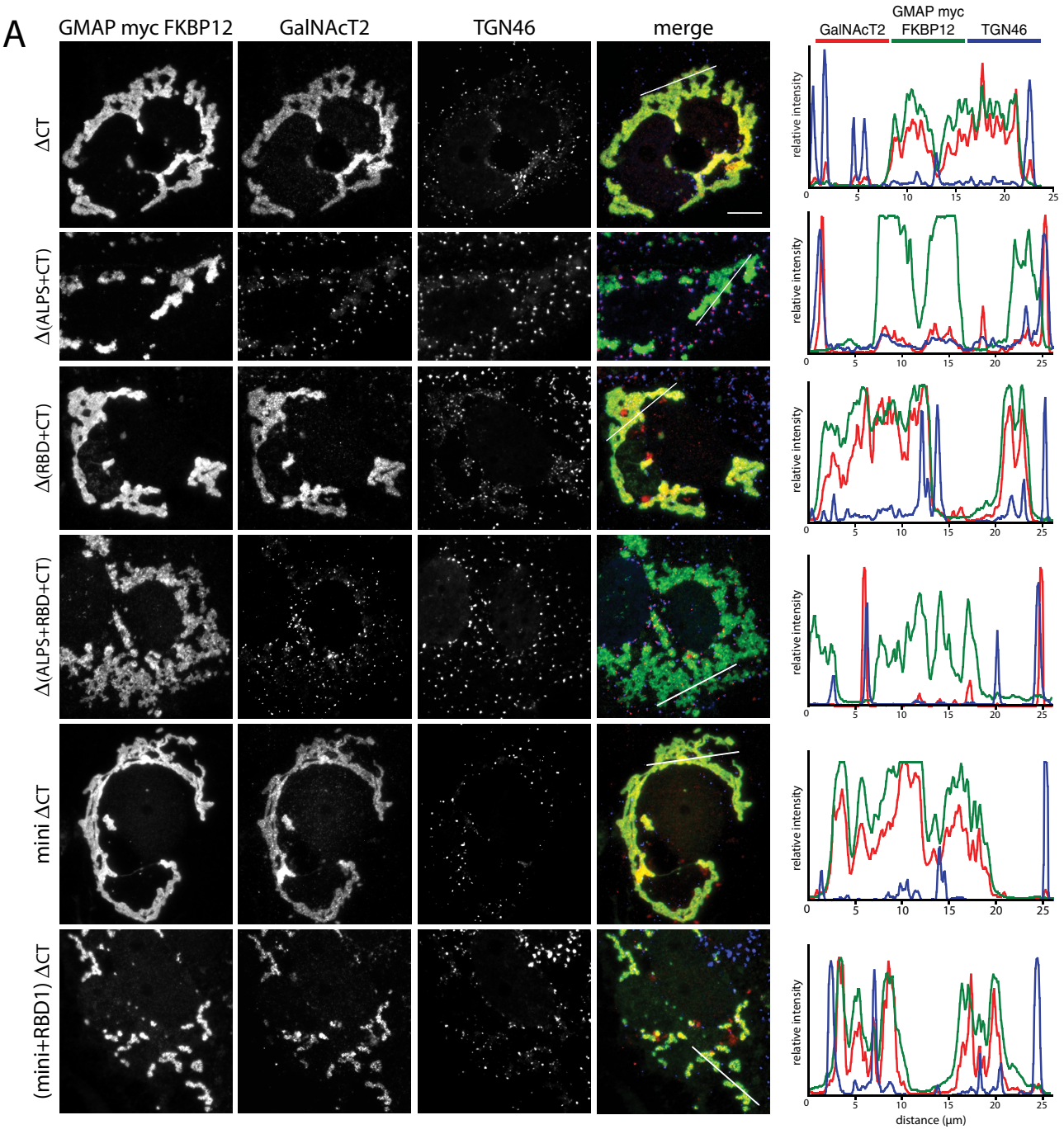
A
GMAP myc FKBP12
GalNAcT2
TGN46
merge
GMAP myc
GalNAcT2
FKBP12
TGN46
ΔCT
Δ(ALPS+CT)
Δ(RBD+CT)
Δ(ALPS+RBD+CT)
mini ΔCT
(mini+RBD1) ΔCT
relative intensity
distance (μm)

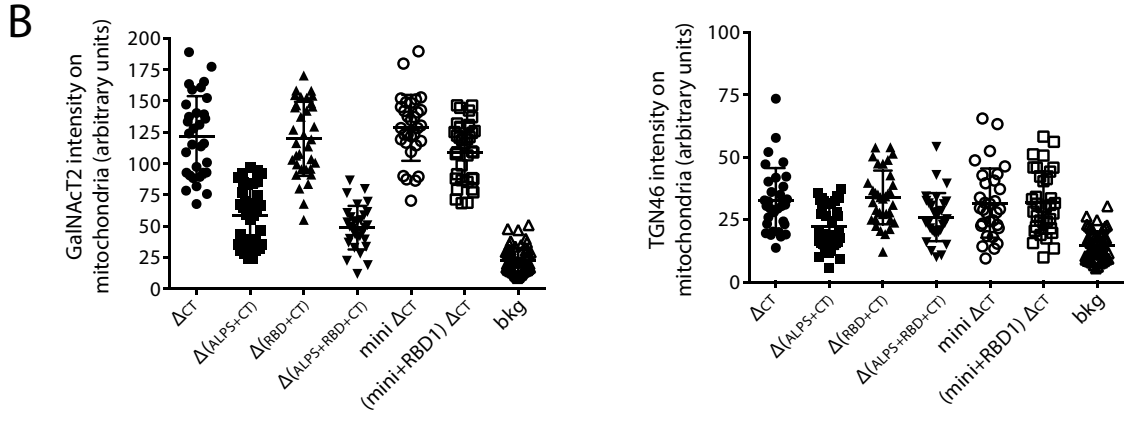
B
GalNAcT2 intensity on mitochondria (arbitrary units)
TGN46 intensity on mitochondria (arbitrary units)
ΔCT
Δ(ALPS+CT)
Δ(RBD+CT)
Δ(ALPS+RBD+CT)
mini ΔCT
(mini+RBD1) ΔCT
bkg

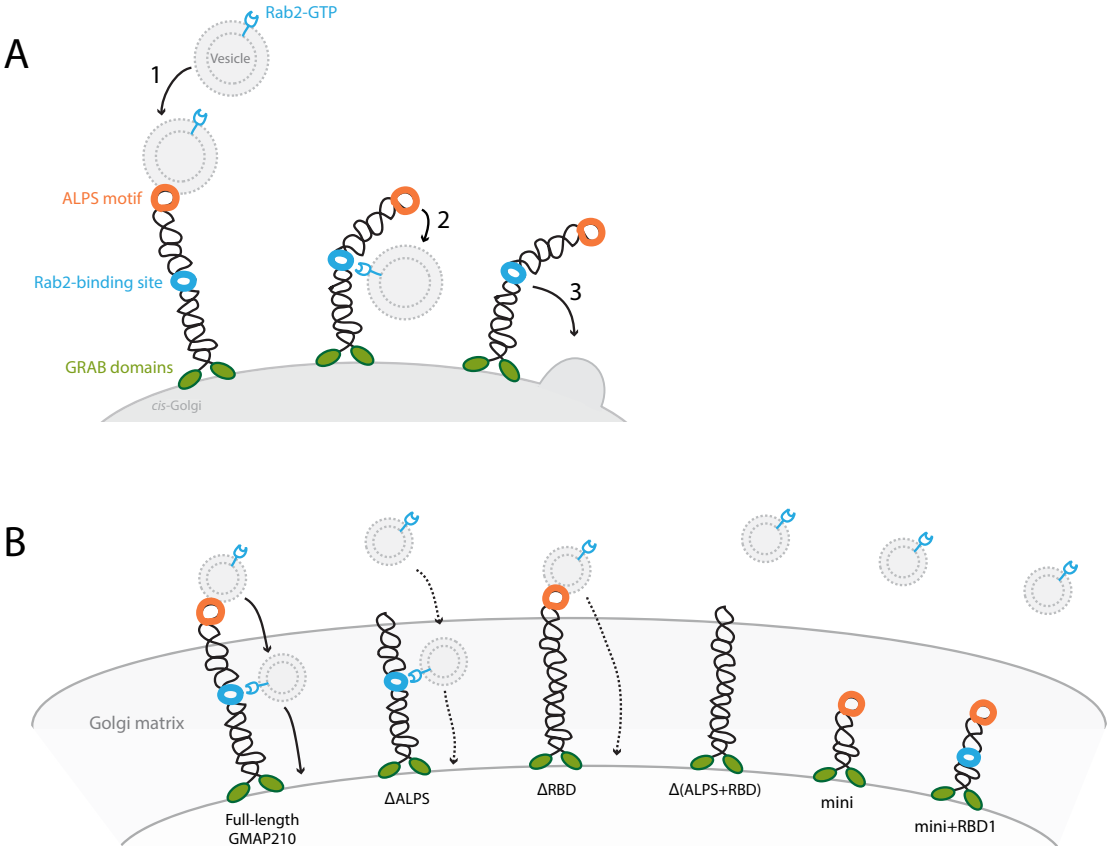

FIGURE 10: Model for GMAP-210–mediated tethering at the Golgi apparatus. See the text for discussion.

was a gift from Henrik Clausen (University of Copenhagen, Copenhagen, Denmark). Mouse monoclonal anti-TfR was purchased from Invitrogen (Paisley, United Kingdom). Mouse anti-p115 (4H1) was described previously (Diao *et al.*, 2003). Rabbit polyclonal anti-Sec24C was a gift from David Stephens (University of Bristol, Bristol, United Kingdom). Antibodies to GM130, golgin-84, GFP, and OCRL1 were described earlier (Diao *et al.*, 2003; Choudhury *et al.*, 2009). Antibodies to GORAB were raised against GST-tagged recombinant GORAB and affinity purified on the recombinant protein. Sheep anti-GRASP65 was a generous gift from Jon Lane (University of Bristol). Sheep anti-GST and anti-TGN46 were described previously (Hyvola *et al.*, 2006). Fluorophore-conjugated secondary antibodies for microscopy and Western blotting were purchased from Life Technologies (Paisley, United Kingdom) and LI-COR Biosciences (Cambridge, United Kindom), respectively, and horseradish peroxidase–conjugated antibodies were bought from Tago Immunologicals (Burlingame, CA).

Constructs

All constructs were made using standard molecular biology techniques. The sequence encoding full-length human GMAP-210 was amplified by PCR from cDNA provided by Francis Barr and inserted in-frame between the *Kpn*I and *Not*I sites of pcDNA5/FRT/TO vector (Life Technologies) for insertion of a Myc-tag at the 3′ end of the sequence. To make the GMAP-210-Myc-FKBP constructs, the FKBP fragment was inserted into pcDNA5-GMAP-210-Myc using *Xho*I. GMAP-210 resistant to siGMAP #2 was generated by introducing six silent mutations by site-directed mutagenesis. Full-length and truncated GMAP-210 sequences were also subcloned into pEGFPC2 (Clontech, Saint-Germain-en-Laye, France), pGAD-T7 (BD Biosciences), and pMAL-C2 (New England Biolabs, Hitchin, United Kingdom) for mammalian expression, yeast two-hybrid analysis, and bacterial expression, respectively. Primer sequences and detailed cloning information for all manipulations are available upon request. Plasmids harboring Rab genes used in GST pull-down and yeast two-hybrid assays were previously described (Hyvola *et al.*, 2006). HRD1-Myc was a generous gift from Stephen High (University of Manchester, Manchester, United Kingdom), and Mito-FRB was a kind gift from Stephen Royle (University of Warwick, Warwick, United Kingdom).

Cell culture, transfections, and treatments

HeLa, HeLa M, HEK293T, and COS7 cells were grown at 37°C and 5% CO_2 in DMEM supplemented with 10% HyClone fetal bovine

FIGURE 9: The ALPS motif is required for GMAP-210-mediated tethering of intra-Golgi vesicles. (A) COS7 cells coexpressing the indicated truncated mutants of GMAP-210-Myc-FKBP along with Mito-FRB were treated with nocodazole for 2 h before induction of mitochondrial relocation with rapamycin for a further 3 h. Cells were costained for the Myc epitope (green), GalNAcT2 (red), and the *trans*-Golgi marker TGN46 (blue). The white line indicates the pixels used for the RGB fluorescence intensity profile plots depicted on the right. Scale bar, 10 μm. (B) Quantitation of mean intensity of GalNAcT2 signal and TGN46 signal within the Myc-positive mitochondrial segments or whole cell (background). Error bars show SD; $n \geq 30$ cells per GMAP-210-Myc-FKBP truncated mutant.

serum (FBS; Thermo Scientific, Altrincham, United Kingdom) and 1 mM L-glutamine. HeLa cells stably expressing GFP-GalNAcT2 (Brian Storrie, University of Arkansas for Medical Sciences, Little Rock, AK) were maintained in the presence of 0.5 mg/ml G-418 sulfate. Transient transfection of plasmid DNA was performed using linear polyethylenimine (PEI; Sigma-Aldrich) or polyethylenimine Max (PEI-Max; Polysciences, Eppelheim, Germany) by forming complexes of DNA:PEI or PEI-Max (1 mg/ml) at a ratio of 1:3, and cells were assayed 24–48 h posttransfection. For the vesicle-tethering assay, COS7 cells were treated with 1 μM rapamycin for 3 h to induce targeting of GMAP-210-Myc-FKBP species onto mitochondrial outer membranes. In some experiments, cells were incubated with 2.5 μg/ml nocodazole for 2 h before and during the rapamycin treatment.

RNA interference

Cells were transfected with 20 nM siRNA duplexes using INTERFERin (Polyplus Transfection, Nottingham, United Kingdom) according to the manufacturer's instructions and were typically analyzed 72 h posttransfection. When cells were additionally transfected with an siRNA-resistant construct during the knockdown, the DNA transfection was carried out 48 h after siRNA transfection. Cells were incubated for additional 24 h and then they were trypsinized, reseeded onto coverslips or glass-bottom dishes, and assayed after another 24 h. GMAP-210 ON-TARGETplus SMARTpool (pool of four siRNAs; L-012684) and each individual ON-TARGETplus siRNA targeting GMAP-210 were from Dharmacon (Thermo Scientific). The sequences of the siRNA oligonucleotides used in this study are siGMAP 1, GGAGAUAGCAUCAUCAGUA; siGMAP 2, CAAGAACAGUUGAAUGUAG; siGMAP 3, GGACAUUACUAAAGAGUUA; and siGMAP, 4, GGGCAAGACUGGAGAGUUA. Luciferase siRNA (GL2; Eurogentec, Southampton, United Kingdom) was used as negative control. Unless indicated otherwise, the results shown were obtained using siGMAP #2.

Immunofluorescence microscopy

Cells plated on coverslips were fixed with 3% (vol/vol) formaldehyde in phosphate-buffered saline (PBS) for 20 min at room temperature and then permeabilized with 0.1% (vol/vol) Triton X-100 for 4 min. Coverslips were washed with PBS, and primary and secondary antibody incubations were performed in PBS with 0.5 mg/ml bovine serum albumin (BSA) at room temperature for 20 min each. The DNA dye Hoechst 33342 was included during the incubation with the secondary antibodies. For labeling the microtubules and actin cytoskeleton, cells were fixed and permeabilized in ice-cold methanol for 4 min before staining with anti–α-tubulin (Viki Allan, University of Manchester) and Alexa 488–phalloidin (Life Technologies), respectively. Coverslips were mounted in Mowiol 4-88 and analyzed using an Olympus BX60 upright microscope equipped with a MicroMax cooled, slow-scan charge-coupled device camera (Roper Scientific, Trenton, NJ) driven by Metaview software (University Imaging Corporation, West Chester, PA). Images were processed using Adobe Photoshop CS5 or ImageJ (National Institutes of Health, Bethesda, MD) software. To assess the recruitment of Golgi proteins to mitochondria, plots of fluorescence intensity versus distance were generated using the RGB profile plot function of ImageJ. To quantify accumulation of Golgi proteins on mitochondria, the mitochondria of transfected cells were segmented by Myc staining, and mean fluorescence intensities of the indicated Golgi proteins within the mitochondria segment were obtained as arbitrary values. Image acquisition settings were kept constant, and analysis was performed on raw images in which the brightness and contrast were adjusted identically. Background fluorescence was measured by quantifying mean fluorescence intensities within whole-cell segments.

Fluorescence recovery after photobleaching

FRAP experiments were performed using a Leica TCS SP5 confocal microscope. Cells were plated in a glass-bottom dishes (MatTek, Ashland, MA), and the medium was changed with CO_2-independent DMEM supplemented with 10% FBS just before FRAP analysis. FRAP was carried out at 37°C using FRAP WIZARD of the LAS AF application. GFP-GalNAcT2 was imaged using a 488-nm laser with a 40×/1.25 numerical aperture (NA) oil immersion objective, and a 1-μm stripe region of interest (ROI) was defined. The ROI was photobleached at a high laser power to result in >80% reduction in fluorescence intensity. Recovery was monitored by measuring fluorescence intensity at 2-s intervals for a total period of 3 min.

Golgi reassembly assay

For the Golgi reassembly assay, cells were treated with 10 μM GCA for 2 h at 37°C. The cells were rinsed five times with warm DMEM to remove any traces of GCA and then incubated in DMEM at 37°C before they were fixed and processed for immunofluorescence or electron microscopy.

Yeast two-hybrid analysis

Yeast two-hybrid experiments were performed as described previously (Diao *et al*., 2003; Hyvola *et al*., 2006).

GST pull-down assay for Rab binding

Cells were solubilized on ice in HNMT buffer (20 mM 4-(2-hydroxyethyl)-1-piperazineethanesulfonic acid [HEPES]–NaOH, pH 7.5, 100 mM NaCl, 5 mM $MgCl_2$, 0.1% Triton-X100) supplemented with protease inhibitors, and lysates were clarified by centrifugation at 13,000 rpm. Postnuclear supernatant containing 2 mg of total protein was mixed with glutathione Sepharose-4B beads (GE Healthcare, Hatfield, United Kingdom) loaded with either GST or 200 μg of a GST-Rab protein. The mixture was rotated for 2 h at 4°C in the presence of 1 mM dithiothreitol (DTT) and either GMP-PNP (for constitutively active, GTP-locked mutants) or GDP (for dominant-negative, GDP-locked mutants). Beads were washed three times with HNMT buffer, and bound proteins were extracted by shaking in extraction buffer (20 mM HEPES-NaOH, pH 7.5, 1 M NaCl, 20 mM EDTA, 0.25% Triton-X, 1 mM DTT) for 20 min at room temperature. After a short spin, the supernatant was precipitated with 10% trichloroacetic acid and resuspended into SDS–PAGE sample buffer. Bound and input proteins were subjected to SDS–PAGE and chemiluminescent or infrared Western blotting.

Electron microscopy

Conventional electron microscopy was carried out as previously described (Diao *et al*., 2003). For correlative light electron microscopy, cells were plated on glass-bottom dishes with a grid pattern (P35G-1.5-14-C-GRID; MatTek). Cells were fixed with 4% (vol/vol) formaldehyde in PBS for 1 h at room temperature and then permeabilized with 0.1% (vol/vol) saponin in PBS containing 0.5 mg/ml BSA for 10 min. Primary and secondary antibody incubations were performed in PBS supplemented with 0.1% (vol/vol) saponin and 0.5 mg/ml BSA for 1 h each. Cells were observed by light microscopy using Delta Vision (Applied Precision, Issaquah, WA) equipped with a charge-coupled device (CoolSNAP HQ; Photometrics) and a 60×/1.4 NA oil immersion objective. Fluorescence and phase-contrast images of the cells of interest were obtained using SoftWoRx software (Applied Precision) on the DeltaVision system. Selected

cells were further processed for serial section transmission EM as previously described (Mironov and Beznoussenko, 2012). Morphological analyses of membrane profiles were performed as follows. Cisternae were defined as membrane profiles with a length at least four times their width. Vesicular profiles were defined as circular profiles with a diameter of 50–200 nm, and cisternal remnants corresponded to membrane profiles with a length >200 nm but shorter than four times their width. For quantitation of membrane profiles, the number of each category within a 1 × 2 µm rectangular grid was counted manually. From 10 to 25 Golgi areas in several sections from 5–16 cells in at least two independent experiments were examined for each condition. The length of cisternae was determined by measuring the length of a line drawn along the center of the cisterna using the free-hand ruler tool in ImageJ, version 1.42.

Statistical analysis

Two-tailed Student's *t* tests were applied to the data using Prism 6 (GraphPad Software, La Jolla, CA).

ACKNOWLEDGMENTS

We thank all colleagues who kindly provided us with antibodies and reagents (as listed in *Materials and Methods*). We thank Mie Wong and Sean Munro (Laboratory of Molecular Biology, Cambridge, United Kingdom) and Francis Barr (University of Oxford) for sharing unpublished data; Peter March and Steve Marsden for assistance with the University of Manchester's Bioimaging facilities; and Philip Woodman (University of Manchester) for critical reading of the manuscript. This work was supported by Biotechnology and Biological Sciences Research Council Grant BB/I007717/1.

REFERENCES

Allan BB, Moyer BD, Balch WE (2000). Rab1 recruitment of p115 into a cis-SNARE complex: programming budding COPII vesicles for fusion. Science 289, 444–448.

Bigay J, Casella JF, Drin G, Mesmin B, Antonny B (2005). ArfGAP1 responds to membrane curvature through the folding of a lipid packing sensor motif. EMBO J 24, 2244–2253.

Broekhuis JR, Rademakers S, Burghoorn J, Jansen G (2013). SQL-1, homologue of the Golgi protein GMAP210, modulates intraflagellar transport in C. elegans. J Cell Sci 126, 1785–1795.

Cardenas J, Rivero S, Goud B, Bornens M, Rios RM (2009). Golgi localisation of GMAP210 requires two distinct cis-membrane binding mechanisms. BMC Biol 7, 56.

Chabin-Brion K, Marceiller J, Perez F, Settegrana C, Drechou A, Durand G, Pous C (2001). The Golgi complex is a microtubule-organizing organelle. Mol Biol Cell 12, 2047–2060.

Choudhury R, Noakes CJ, McKenzie E, Kox C, Lowe M (2009). Differential clathrin binding and subcellular localization of OCRL1 splice isoforms. J Biol Chem 284, 9965–9973.

Diao A, Rahman D, Pappin DJ, Lucocq J, Lowe M (2003). The coiled-coil membrane protein golgin-84 is a novel rab effector required for Golgi ribbon formation. J Cell Biol 160, 201–212.

Drin G, Casella JF, Gautier R, Boehmer T, Schwartz TU, Antonny B (2007). A general amphipathic alpha-helical motif for sensing membrane curvature. Nat Struct Mol Biol 14, 138–146.

Drin G, Morello V, Casella JF, Gounon P, Antonny B (2008). Asymmetric tethering of flat and curved lipid membranes by a golgin. Science 320, 670–673.

Follit JA, San Agustin JT, Xu F, Jonassen JA, Samtani R, Lo CW, Pazour GJ (2008). The Golgin GMAP210/TRIP11 anchors IFT20 to the Golgi complex. PLoS Genet 4, e1000315.

Friggi-Grelin F, Rabouille C, Therond P (2006). The cis-Golgi Drosophila GMAP has a role in anterograde transport and Golgi organization in vivo, similar to its mammalian ortholog in tissue culture cells. Eur J Cell Biol 85, 1155–1166.

Gillingham AK, Tong AH, Boone C, Munro S (2004). The GTPase Arf1p and the ER to Golgi cargo receptor Erv14p cooperate to recruit the golgin Rud3p to the cis-Golgi. J Cell Biol 167, 281–292.

Haas A, Scheglmann D, Lazar T, Gallwitz D, Wickner W (1995). The GTPase Ypt7p of Saccharomyces cerevisiae is required on both partner vacuoles for the homotypic fusion step of vacuole inheritance. EMBO J 14, 5258–5270.

Hayes GL, Brown FC, Haas AK, Nottingham RM, Barr FA, Pfeffer SR (2009). Multiple Rab GTPase binding sites in GCC185 suggest a model for vesicle tethering at the trans-Golgi. Mol Biol Cell 20, 209–217.

Hurtado L, Caballero C, Gavilan MP, Cardenas J, Bornens M, Rios RM (2011). Disconnecting the Golgi ribbon from the centrosome prevents directional cell migration and ciliogenesis. J Cell Biol 193, 917–933.

Hyvola N, Diao A, McKenzie E, Skippen A, Cockcroft S, Lowe M (2006). Membrane targeting and activation of the Lowe syndrome protein OCRL1 by rab GTPases. EMBO J 25, 3750–3761.

Infante C, Ramos-Morales F, Fedriani C, Bornens M, Rios RM (1999). GMAP-210, A cis-Golgi network-associated protein, is a minus end microtubule-binding protein. J Cell Biol 145, 83–98.

Lee I, Tiwari N, Dunlop MH, Graham M, Liu X, Rothman JE (2014). Membrane adhesion dictates Golgi stacking and cisternal morphology. Proc Natl Acad Sci USA 111, 1849–1854.

Lowe M (2011). Structural organization of the Golgi apparatus. Curr Opin Cell Biol 23, 85–93.

Miller PM, Folkmann AW, Maia AR, Efimova N, Efimov A, Kaverina I (2009). Golgi-derived CLASP-dependent microtubules control Golgi organization and polarized trafficking in motile cells. Nat Cell Biol 11, 1069–1080.

Mironov AA, Beznoussenko GV (2012). Correlative light-electron microscopy a potent tool for the imaging of rare or unique cellular and tissue events and structures. Methods Enzymol 504, 201–219.

Munro S (2011). The golgin coiled-coil proteins of the Golgi apparatus. Cold Spring Harb Perspect Biol 3, a005256.

Nakamura N, Lowe M, Levine TP, Rabouille C, Warren G (1997). The vesicle docking protein p115 binds GM130, a cis-Golgi matrix protein, in a mitotically regulated manner. Cell 89, 445–455.

Ohya T, Miaczynska M, Coskun U, Lommer B, Runge A, Drechsel D, Kalaidzidis Y, Zerial M (2009). Reconstitution of Rab- and SNARE-dependent membrane fusion by synthetic endosomes. Nature 459, 1091–1097.

Pernet-Gallay K, Antony C, Johannes L, Bornens M, Goud B, Rios RM (2002). The overexpression of GMAP-210 blocks anterograde and retrograde transport between the ER and the Golgi apparatus. Traffic 3, 822–832.

Pranke IM, Morello V, Bigay J, Gibson K, Verbavatz JM, Antonny B, Jackson CL (2011). alpha-Synuclein and ALPS motifs are membrane curvature sensors whose contrasting chemistry mediates selective vesicle binding. J Cell Biol 194, 89–103.

Ramirez IB, Lowe M (2009). Golgins and GRASPs: holding the Golgi together. Semin Cell Dev Biol 20, 770–779.

Rios RM, Sanchis A, Tassin AM, Fedriani C, Bornens M (2004). GMAP-210 recruits gamma-tubulin complexes to cis-Golgi membranes and is required for Golgi ribbon formation. Cell 118, 323–335.

Rios RM, Tassin AM, Celati C, Antony C, Boissier MC, Homberg JC, Bornens M (1994). A peripheral protein associated with the cis-Golgi network redistributes in the intermediate compartment upon brefeldin A treatment. J Cell Biol 125, 997–1013.

Rivero S, Cardenas J, Bornens M, Rios RM (2009). Microtubule nucleation at the cis-side of the Golgi apparatus requires AKAP450 and GM130. EMBO J 28, 1016–1028.

Rothman JE (1981). The golgi apparatus: two organelles in tandem. Science 213, 1212–1219.

Saenz JB, Sun WJ, Chang JW, Li J, Bursulaya B, Gray NS, Haslam DB (2009). Golgicide A reveals essential roles for GBF1 in Golgi assembly and function. Nat Chem Biol 5, 157–165.

Shorter J, Warren G (2002). Golgi architecture and inheritance. Annu Rev Cell Dev Biol 18, 379–420.

Sinka R, Gillingham AK, Kondylis V, Munro S (2008). Golgi coiled-coil proteins contain multiple binding sites for Rab family G proteins. J Cell Biol 183, 607–615.

Smits P, Bolton AD, Funari V, Hong M, Boyden ED, Lu L, Manning DK, Dwyer ND, Moran JL, Prysak M, *et al.* (2010). Lethal skeletal dysplasia in mice and humans lacking the golgin GMAP-210. N Engl J Med 362, 206–216.

Wong M, Munro S (2014). Membrane trafficking. The specificity of vesicle traffic to the Golgi is encoded in the golgin coiled-coil proteins. Science 346, 1256898.

Yadav S, Puri S, Linstedt AD (2009). A primary role for Golgi positioning in directed secretion, cell polarity, and wound healing. Mol Biol Cell 20, 1728–1736.